Supplementary Information

Probability of non-exceedance of arsenic concentration in groundwater estimated using stochastic multicomponent reactive transport modeling

Nico Dalla Libera[1], Daniele Pedretti[2*], Giulia Casiraghi[2], Ábel Markó[3], Leonardo Piccinini[4] and Paolo Fabbri[4]

[1] Autorità di bacino distrettuale delle Alpi orientali, Cannaregio 4314, 30121 Venice, Italy (nico.dallalibera@distrettoalpiorientali.it)
[2] Dipartimento di Scienze della Terra "A. Desio", Università degli Studi di Milano (UNIMI), Via Mangiagalli 34, 20133 Milan, Italy (daniele.pedretti@unimi.it; giulia.casiraghi@unimi.it)
[3] József and Erzsébet Tóth Endowed Hydrogeology Chair, Eötvös Loránd University, Budapest, Hungary (marab@student.elte.hu)
[4] Department of Geosciences, Università degli Studi di Padova, Via Gradenigo 6, 35131 Padova, Italy (paolo.fabbri@unipd.it; leonardo.piccinini@unipd.it)
* Correspondence: daniele.pedretti@unimi.it

Contents

SI-1. Datasets, sampling and analyses specifics 2
SI-2. Stratigraphic dataset and transiograms 4
SI-3. Flow model calibration 7
SI-4. Variograms computed on the 2009 dataset 10

SI-1. Datasets, sampling and analyses specifics

The pH, Eh, electric conductivity, temperature and dissolved oxygen were measured by a multiparametric probe (YSI 556 MPS). The ORP was estimated with a platinum electrode and successive automatically corrected to Eh with reference to the standard hydrogen electrode. The Eh values were later converted in pE for geochemical calculations. A flow-through cell was used to measured Eh, to minimize the groundwater exposure to the atmosphere. The chemical parameters were estimated in a laboratory through different standardized methods. Arsenic and manganese were estimated by the UNI EN ISO 17294-2:2005 method, iron was estimated by the APAT CNR IRSA 3160 Man 29 2003 method, ammonium was estimated by the APAT CNR IRSA 4030 A1 Man 29 2003 method, and total organic carbon (TOC) was estimated through the APHA 5310-B 2005 method.

Table S1. Available dataset from the 2009 geochemical survey. X,Y= UTM geographical position (32N); T=temperature; EC = electrical conductivity (µS/cm); ORP =oxidizing-reducing potential; Turb=turbidity. Concentrations as μgL^{-1}.

Nome	X	Y	pH	T	EC	Turb	$O_{2(aq)}$	As	Fe	Mn	B	F
PZP032	2300283	5037034	6.84	16.27	766	0.7	7.4	8	2036	419	86	202
PZP033	2300350	5036929	6.93	17.1	604	1000	24	15	1752	1079	110	514
PZP034	2300601	5037113	6.17	14.48	741	0.69	13.1	6	1451	303	60	516
PZP035	2300475	5036856	6.6	15.83	554	55	9.1	24	1654	177	34	228
PZP036	2300973	5036996	6.86	15.11	826	18	14	1	205	611	98	308
PZP037	2300961	5038217	7.1	15.5	970	1000	12.9	64	3347	263	118	350
PZP038	2300748	5038010	6.86	17.5	2044	2.61	7.2	7	1357	380	77	300
PZP040	2301094	5037814	7.03	17.92	1134	1000	9.1	14	913	348	18	230
PZP041	2301010	5036123	7.93	14.28	643	295	10.4	8	46	216	40	498
PZP043	2301481	5036427	7.76	15.02	711	72	8.1	26	1563	187	86	351
PZP045	2299883	5037414	6.93	15.12	1017	21	8	1	1214	582	396	146
PZP046	2300076	5036916	8.63	13.66	660	286	9.8	17	1682	288	92	315
PZP047	2300700	5037662	6.96	18.17	1141	95	13.4	46	1300	804	107	280
PZP048	2300676	5037289	6.49	15.43	1100	498	9.8	9	4462	419	113	205
PZP049	2301021	5038583	7.09	17.08	786	24.58	8.1	20	819	302	24	230
PZP050	2301127	5038092	7.03	16.15	740	14.73	9.5	55	1439	82	41	350
PZP051	2301045	5037179	7.09	16.7	782	12	14.9	1	690	161	89	222
PZP052	2300955	5036921	6.76	17.12	907	1000	10.8	11	1135	411	62	280
PZP053	2300865	5036277	8.69	13.86	492	6.54	7.3	174	1304	398	27	400
PZP054	2301328	5037011	6.9	15.18	1065	1000	10.7	32	1660	406	932	235
PZP055	2301366	5036100	9.06	14.17	814	71	9.7	142	4700	98	118	335
PZP056	2301656	5037711	6.76	20.66	1277	1000	13.3	15	1334	765	144	260
PZP057	2301696	5037214	8.83	12.16	706	457	32.8	2	10	2.5	65	728
PZP058	2301144	5035770	8.47	13.41	972	52	10.9	142	1508	148	131	372
PZP060	2301685	5038115	8.32	12.98	593	1000	36.8	1	208	71	26	586
PZP061	2301821	5037961	8.34	15.02	2149	1000	7.4	14	367	425	261	779
PZP062	2300313	5037097	7.04	14.41	822	55	18.3	28	1865	235	63	218
PZP063	2300763	5037255	6.68	15.33	1326	75	7.7	4	1199	582	78	299
PZP064	2300975	5037164	8.83	14.09	955	0	28.5	3	64	96	85	366
PZR035	2300478	5036855	6.61	16.59	740	374	16.9	7	645	885	42	230
PZR037	2300962	5038216	6.93	17.71	879	1000	14.3	29	1905	331	53	303

PZR038	2300748	5038013	6.87	20.65	1261	25.01	16.6	2	33	214	132	200
PZS_038	2300748	5038015	7.04	17.58	1067	166	8.6	10	0.765	602	72	200
PZS_040	2301091	5037815	6.96	17.75	1392	1000	8.1	21	1.38	394	52	230

Table S2. Available dataset from the 2017 geochemical survey. T=temperature; EC = electrical conductivity (µS/cm); ORP =oxidizing-reducing potential; TOC = total organic carbon

ID	T	pH	Eh	EC	HCO3	NH4	PO4	SO4	F	Cl
units	°C	pH	mV	µS/cm	mg/L	mg/l	mg/l	mg/l	mg/l	mg/l
PZP036	14.2	7.16	-161	855	539	0.91	0.1	71	0.16	21
PZP038	14.3	6.9	-48.3	904	636	2.3	0.03	1	0.1	26
PZP040	17	7.07	-110.4	886	530	0.15	0.03	31	0.27	34
PZP041	14.3	7.02	-141.2	881	539	3.67	0.14	12	0.13	45
PZP043	15.1	7.1	-100.3	737	477	3.44	0.12	1	0.19	33
PZP053	13.9	7.27	-137.2	611	438	3.5	0.03	1	0.25	15
PZP061	15.8	6.78	-78.9	2432	688	0.12	0.05	1	1.5	135
PZP064	16.2	7.18	-151.3	894	498	0.79	0.34	56	0.19	48

ID	Na	K	Mg	Ca	Si	S	TOC	As	B	Fe	Mn
units	mg/l	mg/l	mg/l	mg/l	mg/l	mg/l	mg/l	µg/l	µg/l	µg/l	µg/l
PZP036	26.5	2.1	31.6	135.6	5.15	0.05	3	3	78	1257	162
PZP038	28.2	2.5	42.2	129.2	9	0.05	2.9	11	28	3222	159
PZP040	18.9	0.8	45.1	119.7	7.45	0.05	1.5	17	14	1464	168
PZP041	33.9	2.4	34.1	118.6	10.5	0.05	3.4	16	77	2245	195
PZP043	30.2	2.4	31.2	92.4	8.8	0.05	3.7	29	48	1391	119
PZP053	9.8	7.5	23.7	91.4	10.82	0.05	2	126	21	1441	153
PZP061	151.6	2.7	137	294	8.5	0.05	5	8	251	1240	696
PZP064	35.8	7.2	29	128.6	5.03	0.05	2.6	14	65	2779	370

SI-2. Stratigraphic dataset and transiograms

The subsurface lithological model was generated using the stratigraphic logs from the publicly available borehole database managed by the Veneto Region (http://gisgeologia.regione.veneto.it/website/dati_sond/viewer.htm). Some119 boreholes within the WAA were accounted for during the spMC analysis. Their spatial distribution is shown in Figure S1a. Two cross-sections A-A' and B-B' are shown respectively in Figure S1b and S1c; the sections are respectively parallel of the x and y directions.

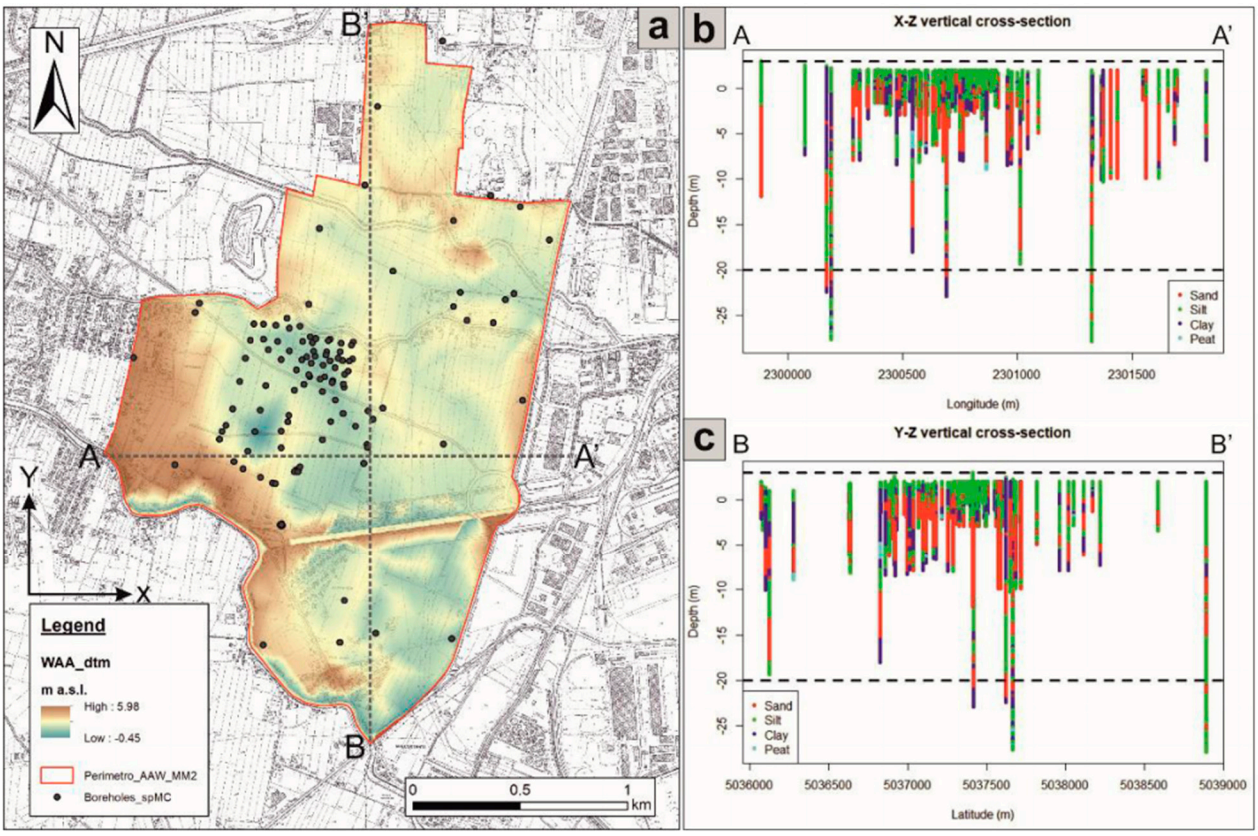

Figure S1. (a) Spatial distribution of boreholes used for subsurface heterogeneity modeling of WAA. (b) and (c) show two cross-sections along X and Y direction respectively with a depth (z) discretization of 0.1 m.

The stratigraphic logs reached a maximum depth of 20 meter below the ground level, which comprises the 12-m-thick sediments modelled in this work. The boreholes data were reclassified in-house into four material classes: "Sand", "Silt", "Clay", "Peat". They were then discretized along the vertical (z) direction with a discretization of Δz=0.1m. The classification and discretization process were developed through a C++ script that recognizes the materials along the depth direction and reassigns them to the new discretized depth information.

Table S3 summarizes the embedded transitional probabilities (TPs) computed by spMC for each material along the three Cartesian direction (x, y, z). The associated transiogram map is depicted in **Figure S2**, while Figure S3 reports the transiograms along the depth direction. The results suggest that there is a clear transition or trend of "silt" and "clay" materials along the x and y directions (higher TPs), as emphasized by This result agrees well with the depositional trend of a flood plain environment. On the contrary, the TPs associated to the "peat" material suggest a more limited and erratic occurrence of this material in the WAA. Along the vertical direction, the "sand" and "silt" materials have a winder transition lag than the other materials. "Peat" material, instead, have small transition lags repeated along the depth, as revealed by the oscillation of experimental

transiogram. This means that “peat” materials may be located in thin layers stack on top of each other and randomly distributed in the aquifer.

Table S3. Embedded transitional probabilities along x, y and z direction.

TP along x	Sand	Silt	Clay	Peat
Sand		0.72	0.28	0.00
Silt	0.55		0.42	0.03
Clay	0.46	0.54		0.00
Peat	0.00	0.76	0.24	

TP along y	**Sand**	**Silt**	**Clay**	**Peat**
Sand		0.67	0.32	0.01
Silt	0.58		0.41	0.01
Clay	0.32	0.54		0.06
Peat	0.61	0.76	0.09	

TP along z	**Sand**	**Silt**	**Clay**	**Peat**
Sand		0.63	0.35	0.02
Silt	0.49		0.50	0.01
Clay	0.22	0.74		0.04
Peat	0.00	0.71	0.29	

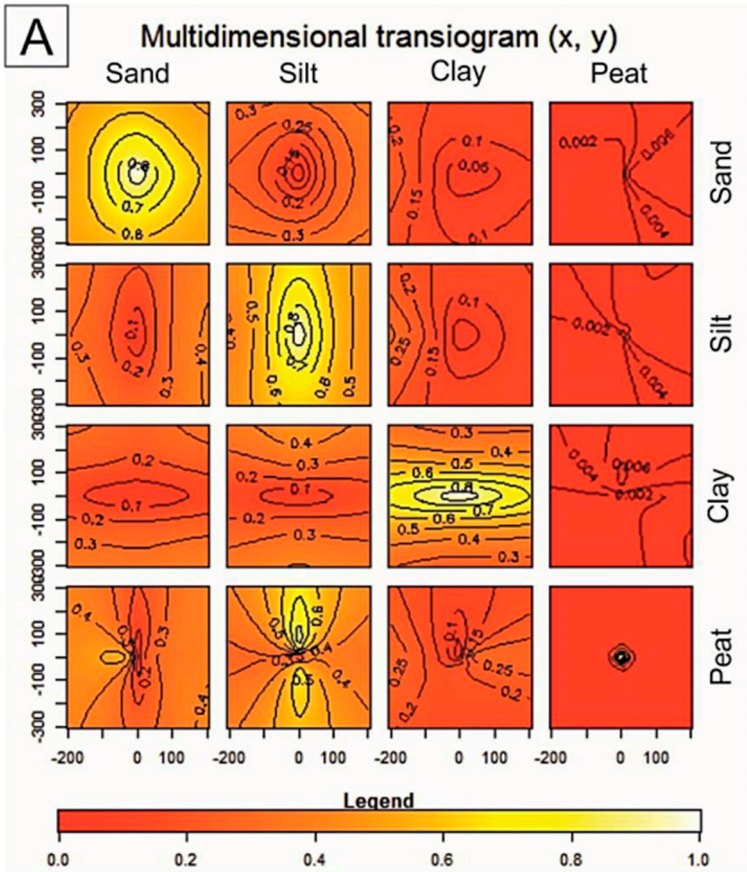

Figure S2. Multidimensional transiograms along x and y direction. The color ramp describes the magnitude of the transitional probability [0,1].

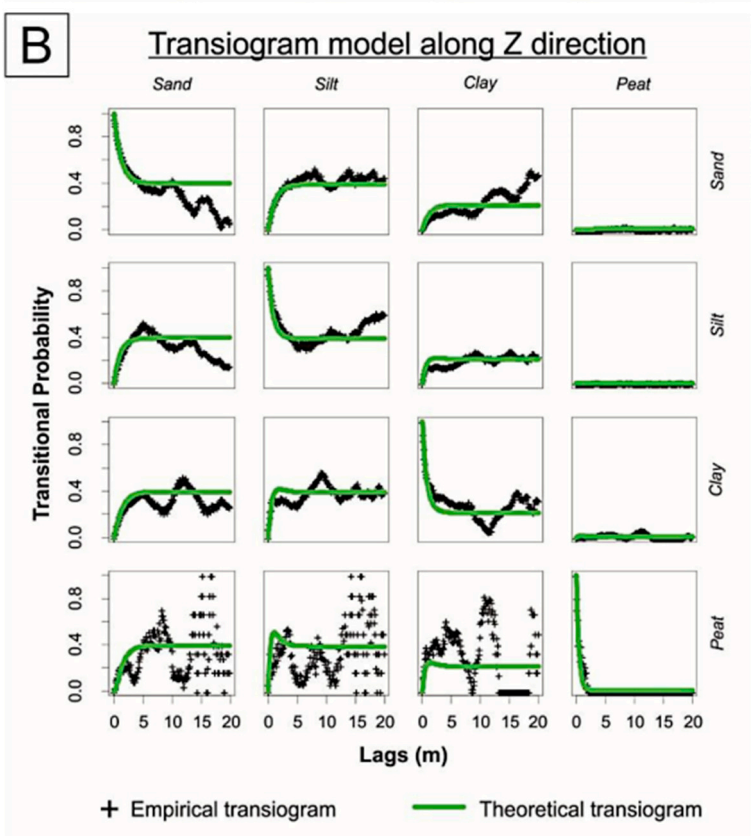

Figure S3 Transiogram along the z direction, illustrating the vertical stratification of the four analyzed materials.

SI-3. Flow model calibration

For each material, initial sets of K, S_S and S_y were obtained from slug tests performed in a few boreholes in the WAA. An example of slug test and its interpretation to estimate hydraulic parameters is shown in Figure S4.

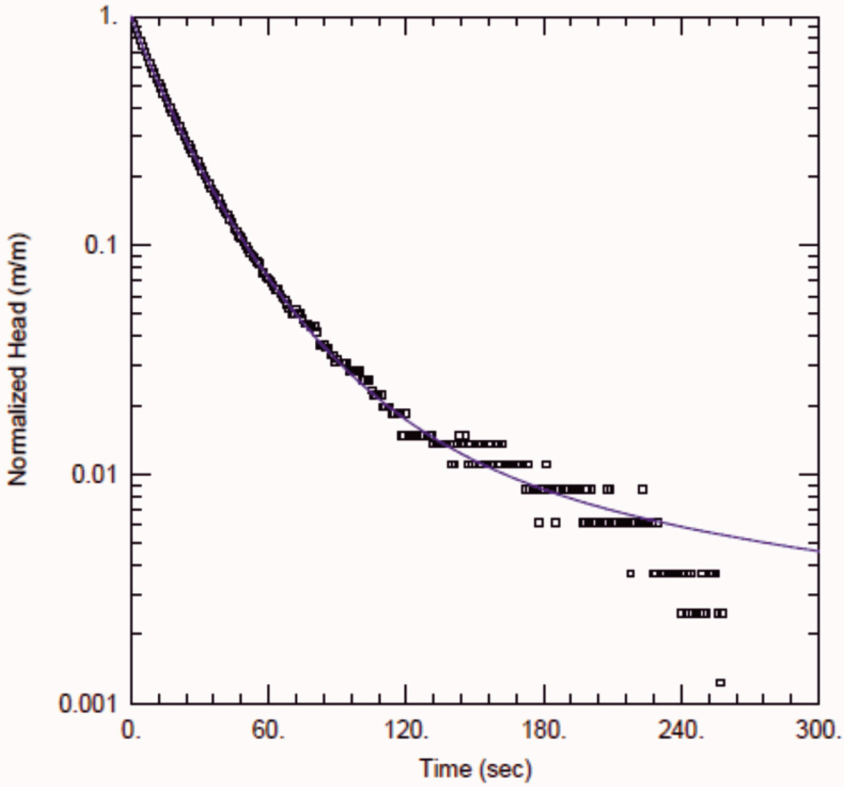

WELL TEST ANALYSIS

Data Set: C:\Users\Utente\Desktop\TESI\pzp_041_slug\pzp_041_slug.aqt
Date: 04/04/18 Time: 16:19:04

PROJECT INFORMATION

Company: tesi magistrale
Test Well: pzp_041
Test Date: 23/11/2017

AQUIFER DATA

Saturated Thickness: 3. m Anisotropy Ratio (Kz/Kr): 0.1

WELL DATA (pzp_041)

Initial Displacement: -0.814 m Static Water Column Height: 4.757 m
Total Well Penetration Depth: 3. m Screen Length: 3. m
Casing Radius: 0.055 m Well Radius: 0.076 m

SOLUTION

Aquifer Model: Confined Solution Method: Cooper-Bredehoeft-Papadopulos
T = 0.0006239 m^2/sec S = 6.64E-7

Figure S4 Example of slug test: on top, the observed head levels and the best fitted model; below, the resulting statistics.

Since PHAST is not directly coupled to an automatic calibration algorithm, the flow model was first calibrated through a manual "trial-and-error" approach. Then, an independent automatic calibration was performed using the codes MODFLOW-2005 (Harbaugh, 2005) and PEST (Doherty *et al.*, 1994), providing similar results as the manual calibration (results not reported). Calibrated parameters were K, S_S and S_y and the transient recharge rate of the RCH boundary conditions. Porosity was set to ϕ=0.25, a typical value for sandy aquifers, and not calibrated. A first-cut estimate of the recharge rate was obtained considering a fraction of the daily rainfall depths recorded in the closest weather station and located in the city of Mira (about 7 km far from the center of the modelled area) (Figure S5). The dataset was provided by Environmental protection Agency of Veneto Region (ARPAV).

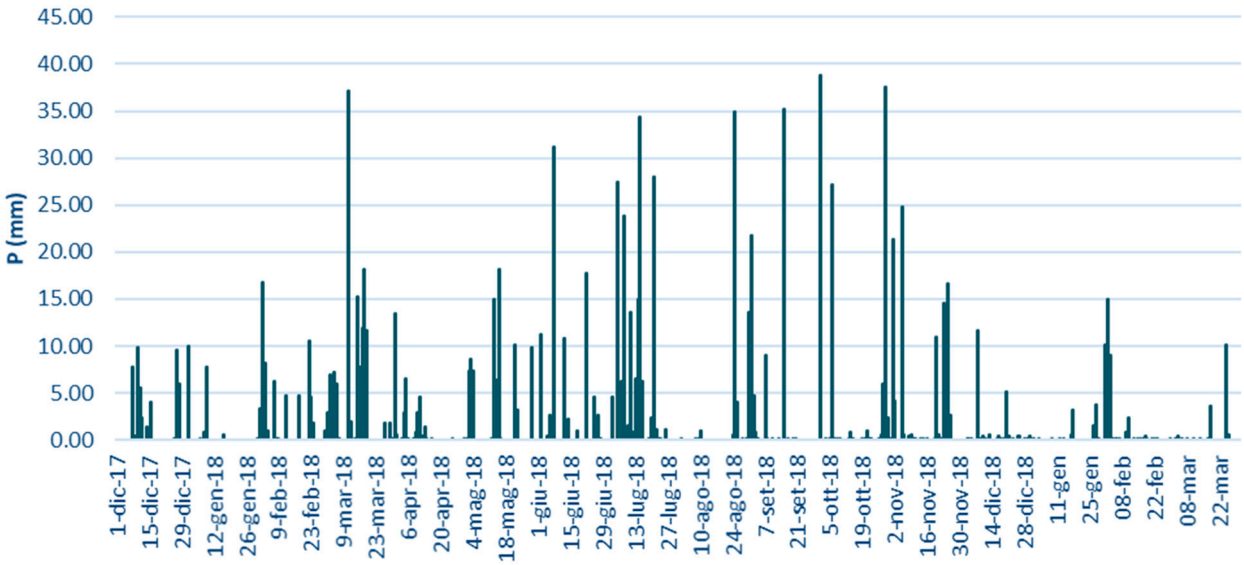

Figure S5 Daily rainfall time series provided by the Environmental Protection Agency of Veneto Region (ARPAV). The rainfall depths were measured at the weather station located in the city of Mira.

The accuracy of the flow model calibration process was evaluated by matching simulated and observed hydraulic heads in reference boreholes. Specifically, the continuous logs of hydraulic heads collected at PZP36, PZP40 and PZP41 during the experimental campaigns presented in Dalla Libera *et al.* (2020) were used as calibration targets. These monitoring wells are located respectively located in the middle, northern and southern zones of WAA, therefore providing a reference head values in distinct parts of the aquifer.

The obtained results are shown in Figure S6. The implemented numerical model is able to reproduce the mean head levels in the three reference piezometers. An average efficiency index NSI, evaluated through the Nash-Sutcliffe method (Moriasi *et al.*, 2007) resulted in $NSI = 0.33$, i.e. a "reliable" calibration. In the middle part of WAA, the match between simulated and observed head levels at PZP36 is less accurate than at PZP40 and PZP41. This is explained considering that PZP36 is closer to the drainage system than the other piezometers. Using this mesh discretization, the simulated PZP36 head levels are more controlled by the DRN boundary than they are in real life. While a higher mesh refinement could have likely improved the head response in the PZP36 model cell, such a higher refinement may result in larger computational time. Since the main purpose of this model was to perform Monte-Carlo MRTM simulations to obtain a regional (i.e. model-wide) response of the aquifer, we considered the achieved level of calibration as sufficient good for the sake of this modelling analysis, and the adopted grid resolution as a proper trade-off between computational efficiency and ability of the model to reproduce the most salient hydrological features.

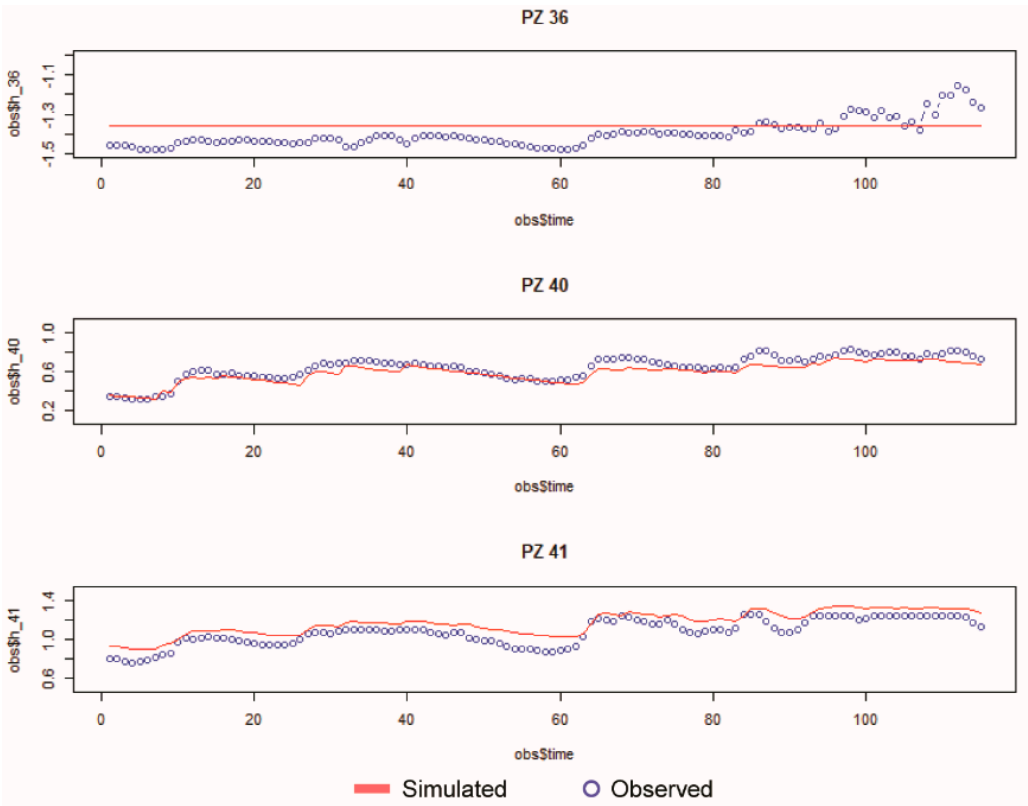

Figure S6 Comparison between the observed data collected through the weekly monitoring and the simulated data obtained by the 3D flow model. Both datasets are expressed using a daily lag time.

To further corroborate the quality of the calibration process, we visually compared the planar view of the resulting piezometric distribution in the aquifer at time 115 days (Figure S7 – left) and interpolated map of the head levels for the same period of time (right). Note that the two maps are similar, both in terms of variability in calculated head values and in the presence of the central depression caused by the drainage system.

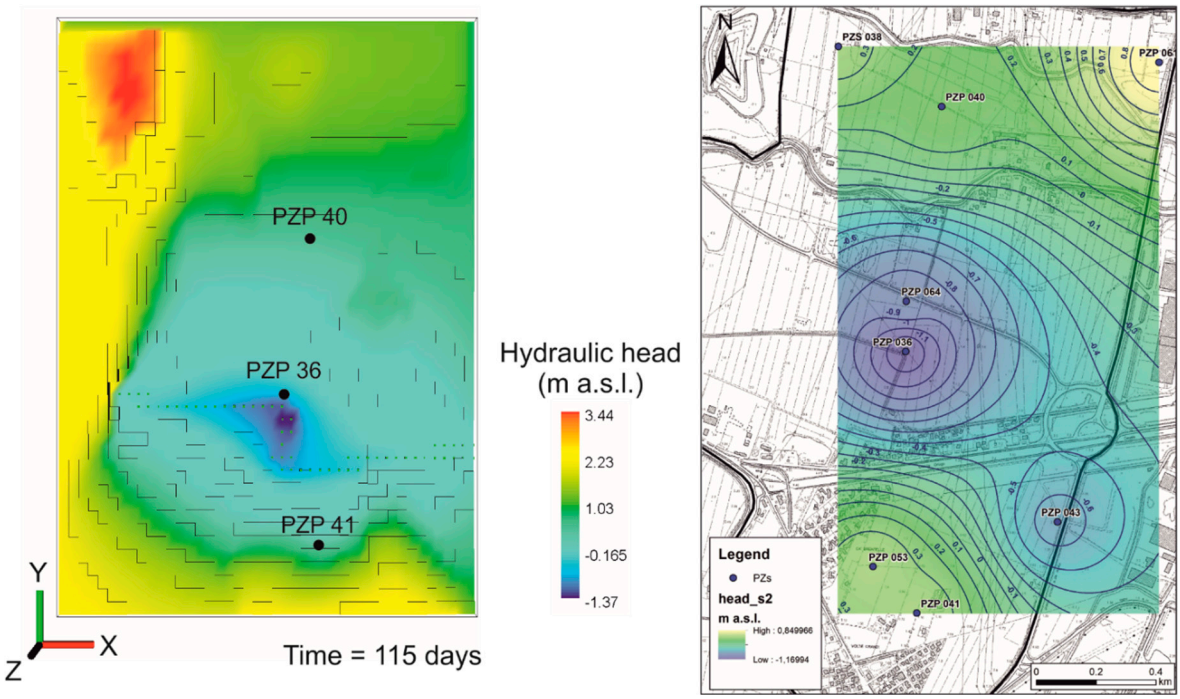

Figure S7 Comparison between the hydraulic head distribution simulated through the 3D flow model in PHAST and the hydraulic head map obtained from the interpolation of the data collected during the surveys.

SI-4. Variograms computed on the 2009 dataset

The variograms were calculated using the code SGEMS v2.1 (http://sgems.sourceforge.net/ , last accessed 8 August 2021) and reported below for As and Fe, respectively. We assumed an isotropic single-structure exponential model, with covariance (*C*) function of form

$$C(X) = C_0 + \sigma_X^2 \exp\left(-\frac{d}{a_X}\right)$$

where X is the variable, C_0 is the nugget effect, σ_X^2 is the sill (or variance), *d* is the lag distance and a_x is the range, which is related to characteristic correlation lengths. An average lag distance of 100m, with a tolerance of 100m, was considered.

- *X*=log(As), C_0=0.05, σ^2=0.4, a=1000m

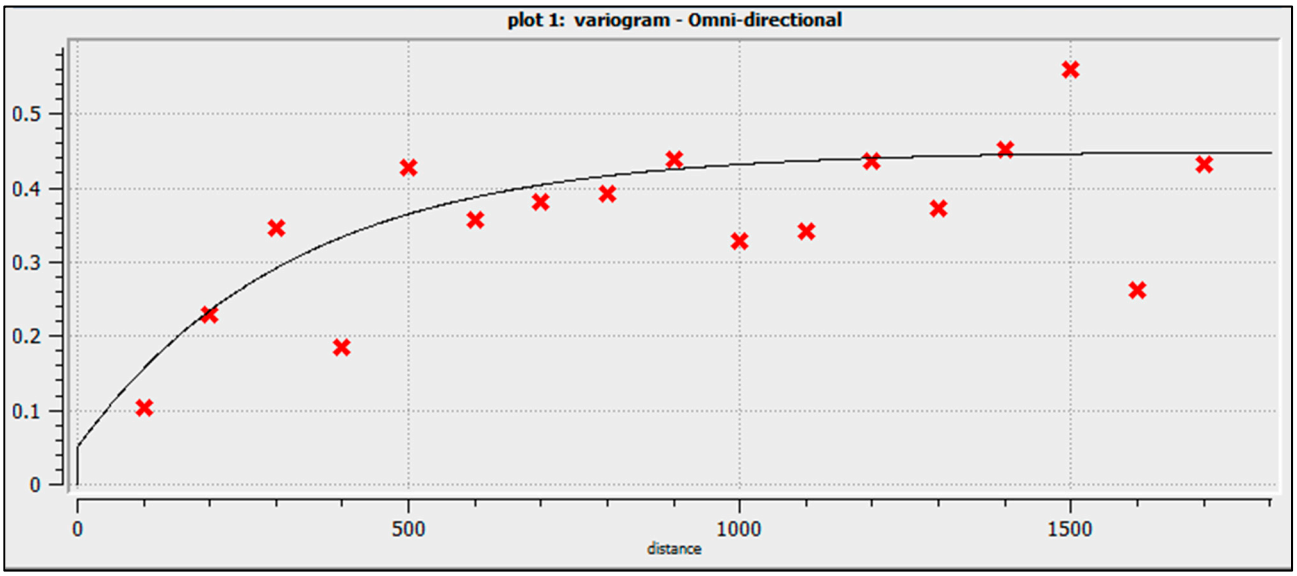

- *X*=log(Fe), C_0=0.05, σ^2=0.5, a=600m

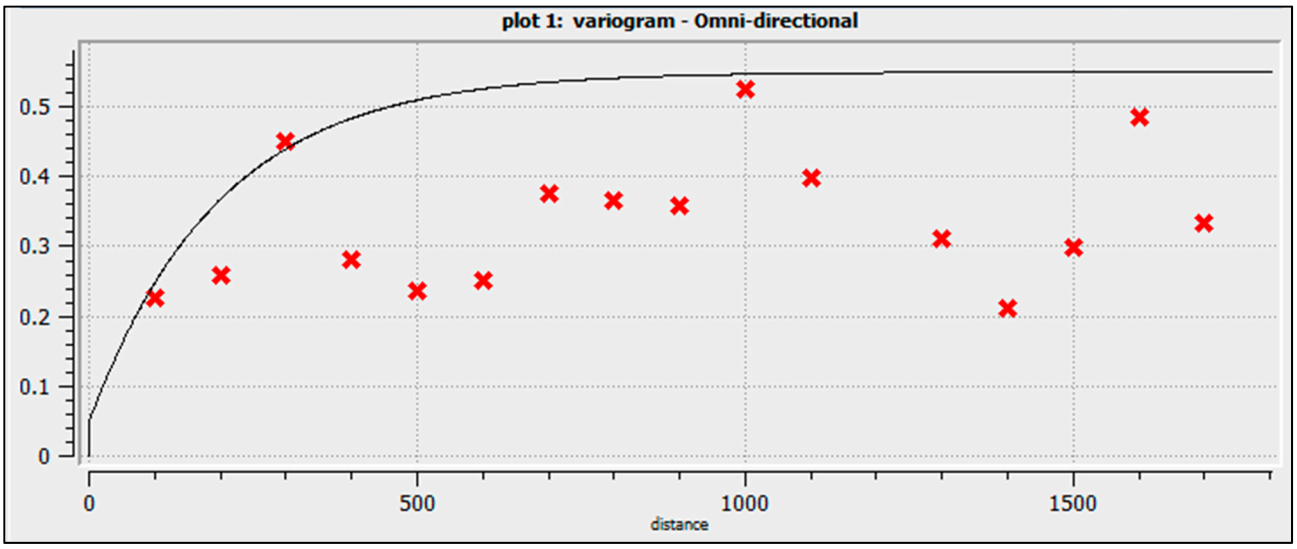

Examples of two SIS realizations reproducing As spatial variations in the modeled area are shown in Figure S8. The white line represents the WAA boundary. The realizations were obtained after backtransforming the data from log to linear scales. Note that the maximum concentration is 174 μgL^{-1}, matching the maximum concentration measured in 2017 (see section SI-1). Similar maps are produced for Fe.

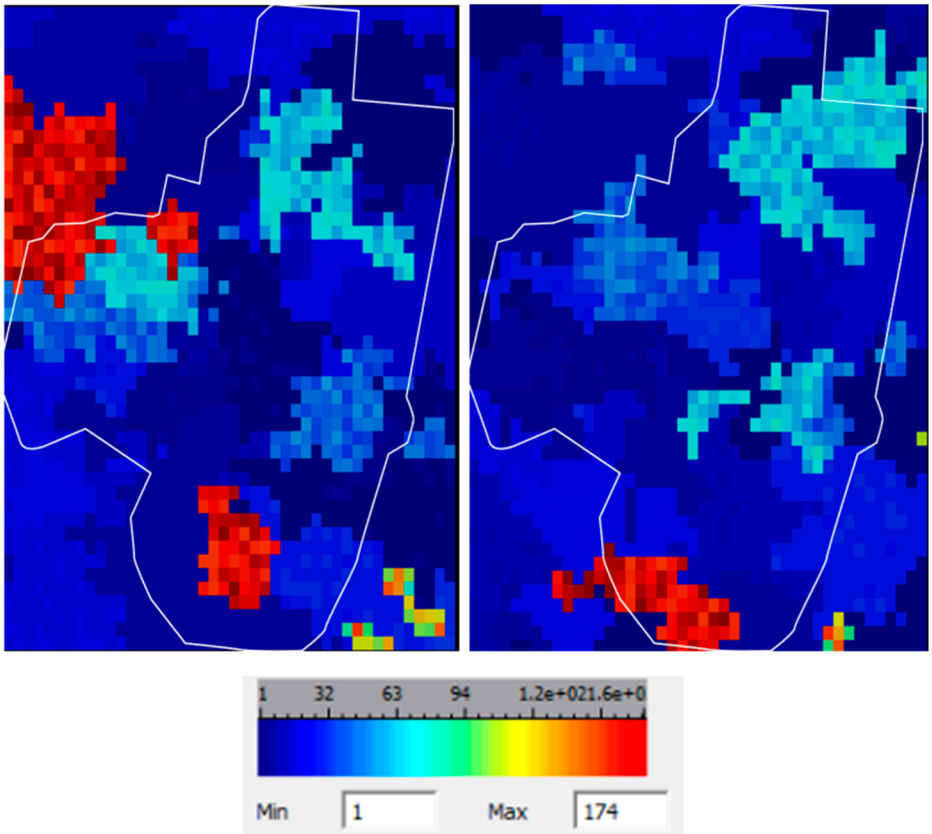

Figure S8 Two SIS realizations generated using SGEMS representing the variation of arsenic concentrations. The maps are created using the variograms presented above and calculated on the 2009 dataset, but conditioned to the 2017 measured concentrations in the eight monitored piezometers.

Bibliography:

Dalla Libera N, Pedretti D, Tateo F, Mason L, Piccinini L, Fabbri P. 2020. Conceptual model of arsenic mobility in the shallow alluvial aquifers near Venice (Italy) elucidated through machine learning and geochemical modeling. *Water Resources Research*, 56(9): e2019WR026234. https://doi.org/10.1029/2019WR026234.

Doherty J, Brebber L, Whyte P. 1994. PEST: Model-independent parameter estimation. *Watermark Computing, Corinda, Australia*, 122: 336.

Harbaugh AW. 2005. MODFLOW-2005 : the U.S. Geological Survey modular ground-water model--the ground-water flow process. *Techniques and Methods*.

Moriasi DN, Arnold JG, Van Liew MW, Bingner RL, Harmel RD, Veith TL. 2007. Model evaluation guidelines for systematic quantification of accuracy in watershed simulations. *Transactions of the ASABE*. American society of agricultural and biological engineers, 50(3): 885–900.